Self-Assembled Colloidal Gel Using Cell Membrane-Coated Nanosponges as Building Blocks

Yue Zhang[1,2], **Weiwei Gao**[1,2], **Yijie Chen**[1,2], **Tamara Escajadillo**[3,4], **Ronnie H. Fang**[1,2], **Victor Nizet**[3,4], and **Liangfang Zhang**[1,2,*]

[1]Department of Nanoengineering, University of California San Diego, La Jolla, California 92093, USA

[2]Moores Cancer Center, University of California San Diego, La Jolla, California 92093, USA

[3]Department of Pediatrics, University of California San Diego, La Jolla, California 92093, USA

[4]Skaggs School of Pharmacy and Pharmaceutical Sciences, University of California San Diego, La Jolla, California 92093, USA

Abstract

Colloidal gels that combine oppositely charged nanoparticles are increasingly leveraged for drug delivery and tissue engineering applications. Meanwhile, cell membrane-coated nanoparticles are becoming unique biomimetic nanomedicine for innovative therapeutics. Inspired by the remarkable potential of both platforms, herein we investigate the use of cell membrane-coated nanosponges as building blocks to form colloidal gel. Specifically, we prepare red blood cell membrane-coated nanoparticles (namely 'nanosponges', denoted 'RBC-NPs'). In the presence of appropriate cationic nanoparticles, the nanosponges self-assemble to form a gel-like and cohesive complex (namely 'nanosponge colloidal gel', denoted 'NC-gel'). When applied with an external shear force, the NC-gel shows shear-thinning behavior; however, upon removal of the external force, the cohesive property recovers. The NC-gel not only preserves the toxin neutralization capability of the nanosponges, but also prolongs their retention after subcutaneous injection into mouse tissues. In a mouse model of subcutaneous Group A *Streptococcus* (GAS) infection, the NC-gel shows significant antibacterial efficacy by markedly reducing skin lesion development. Overall, we demonstrate the successful use of cell membrane-coated nanoparticles as building blocks to formulate colloidal gel that entirely based on material self-assembly without chemical cross-linking. The new colloidal gel system is promising as an injectable formulation for therapeutic applications such as antivirulence treatment for local bacterial infections.

Keywords

Colloidal gel; nanosponge; self-assembly; detoxification; bacterial infection

*Correspondence authors: zhang@ucsd.edu.

Introduction

Colloidal gels comprise a continuous network of particles assembled through strong, yet transient and reversible, electrostatic charge interactions.[1–2] With compelling shear thinning and self-healing characteristics, they are becoming an important class of biomaterials with broad applications.[1, 3] Recently, the use of therapeutic nanoparticles as building blocks to formulate colloidal gels is gaining attention in drug delivery and tissue engineering applications.[4–5] Such polymeric nanoparticles have distinct engineering flexibility for tailored physicochemical properties such as size, charge, and surface chemistry; therefore, they offer a simple route to assemble highly tunable gel-like materials while avoiding complex molecular design and synthesis.[6–7] The resulting nanoparticle colloidal gels confer two levels of structural hierarchy, namely the polymer chain network within each nanoparticle and the cross-linked nanoparticle assembly, which together provide advanced control over drug release kinetics.[8] Compared to bulk hydrogel systems, nanoparticle colloidal gels can effectively alleviate mass transport barriers within the gel network without compromising bulk mechanical strength. As a result, these advanced biomaterials exhibit a fast response to local chemical cues for triggered drug release.[9] In addition, colloidal gels made with high concentrations of nanoparticles exhibit pseudoplastic behavior desirable for fabricating moldable and shape-specific materials.[10] Notably, when constructed of biocompatible and biodegradable materials, these colloidal gels have high potential for tissue regeneration.[11] Together, these multiple advantages make nanoparticle-based colloidal gels a promising class of biomaterials.

Multi-functional nanoparticle design for therapeutic applications has made considerable progress in recent years.[12–13] One emerging approach is the use of natural cell membranes to coat synthetic nanoparticle for bio-functionalization.[14–16] In this approach, intact plasma membranes are collected from natural cells and then wrapped onto nanoparticle surfaces. The resulting cell membrane-coated nanoparticles inherit and display natural surface antigens and associated functions while preserving the highly tunable physicochemical properties of synthetic nanomaterials.[17] This 'top-down' fabrication makes it possible to replicate complex biological interfaces present in nature to confer sophisticated nanoparticle functionality without exposure to foreign materials or unfavorable chemical reactions. Following this approach, nanoparticles have been coated with membranes derived from various cell types including red blood cells (RBCs), platelets, cancer cells, leukocytes, and bacteria. [14, 16, 18–20] These biomimetic nanoparticles have inspired a wide range of innovations in areas such as detoxification, drug delivery, and vaccine nanotechnology. [21–23] Interestingly, regardless of their diverse biological identity and functionality, cell membrane-coated nanoparticles in general carry a net negative surface charge inherited from their source membranes. Therefore, they may spontaneously engage electrostatic charge interactions with cationic materials without the needs of further modification.[17, 24] This feature motivated us to hypothesize that cell membrane-coated nanoparticles could be used as building blocks to construct colloidal gels. If so, this conceptual framework will allow creation of novel colloidal gels that combine biomimetic functionalities with cohesive network properties.

To test our hypothesis, we first fabricated RBC membrane-coated nanoparticles (also referred to as 'nanosponges', here denoted 'RBC-NPs') by coating RBC membranes onto polymeric cores made from poly(lactic-co-glycolic acid) (PLGA) (Figure 1A). At the same time, we prepared companion chitosan-functionalized PLGA nanoparticles that possessed a similar size but opposite surface charge (denoted 'Chi-NPs'). Upon mixing, these two oppositely charged nanoparticles self-assembled, forming a cohesive 3D network or 'nanosponge colloidal gel" (denoted 'NC-gel'). When applied with an external shear force, the NC-gel demonstrated shear-thinning behavior; however, upon removal of the external force, its strong cohesive properties recovered. Such reversible network stability is attributable to the transient disruption of inter-particle interactions, indicating a successful colloidal gel formation.

Notably, prior work with RBC-NPs harnessed their capability to absorb and neutralize structurally diverse bacterial pore-forming toxins for therapeutic administration as antivirulence agents.[15, 23, 25] When embedded into covalently cross-linked hydrogels for injection, the RBC-NPs effectively neutralized secreted bacterial toxins to impede the development of local infection.[26] In present study, we fabricate a NC-gel pairing RBC-NPs and Chi-NPs and achieve significantly prolonged retention of RBC-NPs in both biological buffers and mouse subcutaneous tissues without the need for chemical conjugation. In vitro, the NC-gel retained the full capacity to inhibit toxin-induced hemolysis seen with RBC-NPs alone, indicating that the gel formulation preserves the critical biological functionality of the RBC-NPs. In a mouse model of subcutaneous infection with the toxin-producing human bacterial pathogen group A *Streptococcus* (GAS), the NC-gel showed significant therapeutic efficacy, as evidenced by markedly diminished bacterial skin lesion development. In summary, we have successfully used cell membrane-coated nanoparticles as building blocks to formulate a novel NC-gel entirely based on material self-assembly without chemical cross-linking. The new colloidal gel system demonstrated significant potential as an injectable formulation for medical applications including anti-virulence therapy against localized bacterial infection.

Results and discussion

In the study, RBC-NPs (nanosponges) were prepared by coating membranes derived from human RBCs onto PLGA polymeric cores through a sonication process.[27] The resulting RBC-NPs exhibited a hydrodynamic diameter of 150.9 ± 0.8 nm and a surface zeta potential of -22.3 ± 1.7 mV. Meanwhile, to prepare Chi-NPs, an acetone solution containing PLGA was added dropwise into an aqueous solution of chitosan.[28] The subsequent acetone evaporation led to the formation of Chi-NPs with a diameter of 194.3 ± 1.8 nm and a surface charge of 34.2 ± 0.4 mV. Following the preparations, we directly mixed the two oppositely charged nanoparticles at a fixed mass concentration (20 wt%, PLGA polymer content), but varied the mass ratios of the nanoparticle components. Each formulation was examined for its rheological characteristics. In steady flow measurements, nanoparticle suspensions containing RBC-NP or Chi-NP alone showed low viscosity with minimum shear-thinning behavior (Figure 1B). In contrast, a significant increase in viscosity was observed when two nanoparticles were mixed, revealing the occurrence of strong electrostatic charge interactions between the two colloids. Notably, viscosity values measured from the sample

with an equal mass ratio of the colloids (50 wt% of RBC-NP and 50 wt% of Chi-NPs) was slightly lower than that calculated for the sample with a RBC-NP concentration of 30 wt%. This likely reflects the smaller absolute value of zeta potential of negatively-charged RBC-NPs compared to Chi-NPs, which means that a more equivalent overall charge balance is achieved when they are provided in excess.[10]

Viscous mixtures were further examined with dynamic rheological measurements of the storage modulus (G') and the loss modulus (G'') as a function of frequency (Figure 1C). In all three samples, G' exceeded the corresponding G'' over the entire frequency range tested, and both moduli showed weak dependence on frequency, implying the dominance of a gel-like viscoelastic behavior.[29] Results from steady flow and dynamic measurements were consistent: the mixture with higher viscosity also possessed higher values for the corresponding moduli. Overall, the rheological measurements confirmed the gel formation was predominantly mediated by electrostatic charge interactions. For the subsequent studies, we specifically selected an NC-gel that contained equal masses of RBC-NPs and Chi-NPs (50 wt% of each), as this formulation showed both high viscosity and pronounced shear-thinning behavior, while containing a substantial fraction of RBC-NPs as the active component for biodetoxification.

We next characterized the NC-gel to verify its cohesive network properties. Colloidal gels consisting of oppositely charged nanoparticles are known to exhibit pseudoplastic characteristics, which facilitate the formation of materials with defined shapes under static conditions.[8, 10] Indeed, the suspensions of single component RBC-NPs or Chi-NPs were fluid-like, and unable to form a defined 3D structure when placed onto a substrate (Figure 2A). In contrast, the NC-gel retained a freestanding 3D structure, implying a critical function of its internal charge interactions for maintaining the overall cohesive properties of the colloidal assembly. In addition, consecutive acceleration sweeping with a shear force revealed nearly identical viscosity profiles, indicating an excellent recovery of the NC-gel architecture upon the removal of the external shear force (Figure 2B). The NC-gel was also examined for its microscopic morphology. In the study, RBC-NPs and Chi-NPs were labeled with red (DiD) and green (DiO) fluorescent dyes, respectively, and the resulted NC-gel sample examined by laser scanning confocal microscopy (LSCM, Figure 2C). In ambient conditions, the fluorescent imaging showed the two distinct nanoparticle components to be clearly distinguishable, suggesting reduced particle mobility upon the formation of colloidal assemblies. In addition, the green and red signals were evenly distributed, indicating the homogenous mixing of both nanoparticle components. The imaging also revealed long-range ring- and branch-like structures. When zoomed in, a representative fluorescence image shows that the nanoparticle agglomerates were connected to form a porous structure (Figure 2D). To further characterize these microscopic structures, the NC-gel sample was dried and examined under a scanning electron microscope (SEM). The ultrastructure exhibited a porous morphology with nanoparticles linked into loosely organized circular structures (Figure 2E). In a representative zoomed-in image, domains of more tightly packed nanoparticle agglomerates and open pores were seen (Figure 2F). The observed NC-gel morphology, which features mixed agglomerates and pores, also matches previous studies on nanoparticle colloidal gel systems, implying the cohesive nature of NC-gel as a result of the interplay between nanoparticle attraction (agglomerates) and repulsion (pores).[9–10]

Overall, the structural retention under static conditions, excellent shear-thinning behavior, and microscopic characterizations collectively suggest the successful formation of colloidal gel using RBC-NPs as building blocks.

For local administration and treatment, prolonged retention of RBC-NPs by using the gel formulation is desirable. We hypothesized that the electrostatic attractions among oppositely charged nanoparticle building blocks of NC-gel would prolong RBC-NP retention under physiological conditions, and began by examining RBC-NP diffusion out of the NC-gel network *in vitro*. In this study, the NC-gel was formulated with fluorescently-labeled RBC-NPs and loaded into a dialysis chamber equipped with pores of 1 μm in diameter. The release of RBC-NPs was monitored by measuring the fluorescence intensity outside of the dialysis chamber. For comparison, RBC-NPs alone were used as a control. Within 24 h, the NC-gel released $1.3 \pm 1.5\%$ of the total RBC-NPs, a negligible amount compared to $80.8 \pm 11.1\%$ measured from the pure RBC-NP suspension control (Figure 3A). This sharp contrast in nanoparticle release indicates that the NC-gel can effectively immobilize and retain RBC-NPs within its network. We then investigated retention of the RBC-NPs within the gel under *in vivo* conditions. NC-gel samples containing fluorescence-labeled RBC-NPs were injected subcutaneously into the left flank of mice. As a control, samples containing the same quantity of free RBC-NPs were injected to the right flank of the same mice. Following the injection, whole body imaging of the mice revealed the confinement of fluorescence at the injection sites (Figure 3B). In the study, a faster decay of fluorescence intensity was observed at sites injected with free RBC-NPs compared to to sites injected with the NC-gels, indicating a more rapid loss of nanoparticles through diffusion to surrounding tissues. Quantification of the fluorescence intensity showed that nearly 30% of the free RBC-NPs diffused away from the injection site by day 2 and nearly 50% by day 3. In contrast, the NC-gel formulation showed negligible loss of RBC-NPs during the full 3-day testing period (Figure 3C), demonstrating the prolonged retention of RBC-NPs achieved with NC-gel formulation. Compared to previous studies that used acrylate-based hydrogels for nanoparticle encapsulation and retention, the current approach achieves enhanced nanoparticle retention relying entirely on physical self-assembly without any chemical processing.[26, 29]

RBC nanosponges have shown unique capabilities to absorb and neutralize various pore-forming toxins (PFTs). In this study, we selected this property as a functional assay to test whether the NC-gel formulation retained key biological functionality of the entrapped nanosponges. To do so, we selected the well-characterized GAS toxin (SLO) as a model pore-forming toxin, and tested the ability of the NC-gel to inhibit SLO-induced hemolytic activity compared to free RBC-NPs. An SLO concentration of 1 μg/mL was utilized because at this concentration the toxin causes complete cell lysis. Recombinant SLO was mixed with serial dilutions of NC-gel or RBC-NPs prior to mixing with freshly purified human RBCs. As shown in Figure 4A, in both groups, as the concentration of RBC-NP increased, the degree of RBC hemolysis was correspondingly reduced. Specifically, 50% inhibition of hemolysis was achieved with an RBC-NP concentration of approximately 0.25 mg/mL, and a nearly 100% inhibition observed with a RBC-NP concentration of 1 mg/mL. At all tested concentrations, the NC-gel sample showed an inhibition efficiency comparable to that of

free RBC-NPs, suggesting that the NC-gel formulation retains the full neutralization capability of its component RBC-NPs upon gelation.

Neutralization of SLO by NC-gel was further tested *in vivo* (Figure 4B). In the study, SLO toxin was mixed with NC-gel and free RBC-NPs, respectively, and then injected into the loose flanks of the mice. Mice injected with SLO only and PBS, respectively, served as two control groups. At 72 h after injection, mice challenged with SLO alone developed clear skin lesion with characterized by localized edema and inflammation. In contrast, mice injected with the NC-gel and free RBC-NP preparations had healthy appearing skin at the injection site similar to a PBS control group. Skin biopsy sections were further analyzed with histological staining. Mouse skin treated with SLO alone showed intracellular edema within the stratum spinosum, alteration of vascular structure in the dermal layes, obvious erythrocyte extravasation, and keratinocyte necrosis. In contrast, skins treated with NC-gel, RBC-NPs, or PBS alone possessed normal epithelial structures in skin histology without discernible damages; all of these samples showed stratified squamous epithelium with intact fibrous structures and absence of erythrocyte extravasation. Similar complete toxin neutralization effects observed with the NC-gel compared to RBC-NP group *in vivo* further confirm that the neutralization function of RBC-NP is well preserved within the NC-gel formulation.

Finally, to demonstrate the therapeutic potential of the NC-gel, we tested their use as an anti-virulence agent to protect mice from a live subcutaneous bacterial infection. GAS, which elaborates SLO and several other pore forming toxins and proteases[31–32], is a major cause of invasive to skin and soft tissue infection in humans.[30], making it a relevant model to for testing the efficacy of NC-gel in local treatment. Subcutaneous GAS infection was extablished by injecting 2×10^9 CFU bacteria underneath the flank skin of ICR mice, randomized into three groups (n = 6 per group) for treatment with PBS, free RBC-NPs, and NC-gel, respectively. Therapeutic efficacy was evaluated by measurement of the GAS-induced skin lesion.[33–34] On day 1 after the bacterial challenge, all groups developed visible skin lesions of similar size (Figure 5 A,B). However, on days 2 and 3, the mice treated with the NC-gel showed significantly smaller lesions than mice injected with the PBS control of free RBC-NPs. A partial therapeutic benefit of free RBC-NPs compared to the PBS control was seen on day 3. A superior efficacy in lesion reduction observed with the NC-gel verifies its potential as an effective local treatment agent to mitigate tissue damage produced by GAS infection.

The combination of therapeutic nanoparticles with hydrogels has emerged as a novel biomaterial formulation with intriguing and versatile therapeutic application potentials.[5] However, such combinations to date have relied largely on chemical cross-linking to embed and reatin nanoparticles within the gel network. From this perspective, the NC-gel reported herein provides a straightforward and gentle approach to use nanoparticles themselves as building blocks coupled with an entirely physical gelation process. The resulting NC-gel also generates a unique synergy between cell membrane-coated nanosponges and gel-like bulk assembly: while the nanosponges offer unique biomimetic toxin absorption and neutralization, the hydrogel enhance retention of the nanosponges at the site of application (e.g. an infected tissue focus), which focuses localized bioactivity for enhanced efficacy.

Nanoparticles coated with membranes of mammalian cells or bacterial cells possess a negative surface charge; therefore, the approach of NC-gel formulation likely be extended to nanoparticles coated with many other types of cell membranes. Such cell membrane-coated nanoparticles would also be expected to interact with other cationic materials such as polymers and nanofibers for self-assembly and gelation.[6, 35] This powerful platform of material diversity and formulation flexibility make the NC-gel approach broadly applicable.

In summary, this study introduced a framework for using cell membrane-coated nanoparticles to fabricate colloidal gels. RBC-NPs were studied as a model nanoparticle system and paired them with cationic Chi-NPs to formulate a NC-gel. This colloidal gel was optimized by varying the relative composition of the two oppositely charged nanoparticles. The resulting gel effectively retained RBC-NPs within its network without compromising their toxin neutralization capability. In a GAS subcutaneous mouse infection model, mice treated with the NC-gel showed clear reductions in skin lesion development. The reported NC-gel takes advantage of the natural surface charge of cell membrane in general, and this formulation process is expected to be applicable to nanoparticles coated with membranes of other cell types. The formulation process is physical, facile, and chemical-free, hence allowing the NC-gel to retain functionalities without affecting the original functions of the building blocks. The resulting colloidal gel combines the biomimetic functionality from the cell membrane-coated nanoparticles with the cohesive network property from the bulk gel, together opening new opportunities for advanced therapeutic applications.

Experimental section

Materials:

Chemicals including chitosan oligosaccharide lactate (Mw = 5000), dithiothreitol (DTT), and acetone were purchased from Sigma-Aldrich. Fluorophores including 1,1'-dioctadecyl-3,3,3',3'-tetramethylindodicarbocyanine, 4-chlorobenzenesulfonate salt (DiD, excitation/emission = 644/665 nm) and 3,3'-dioctadecyloxacarbocyanine perchlorate (DiO, excitation/emission = 484/501 nm) were purchased from ThermoFisher Scientific. Poly (lactic-*co*-glycolic) acid (PLGA, 50:50, 0.67 dL/g) was purchased from LACTEL Absorbable Polymers. Packed human red blood cells (RBCs) were purchased from ZenBio, Inc., from which cell membrane was derived according to a previously published protocol. [14]

Preparation of RBC membrane-coated nanosponge colloidal gel (NC-gel):

RBC-NPs were synthesized by coating bare PLGA cores with RBC membrane.[27] Briefly, to prepare bare PLGA cores, 10 mL of PLGA (20 mg/mL in acetone) was added to 20 mL of Tris-HCl buffer (10 mM, pH = 8). The solution was stirred and allowed to evaporate for 2 h. For membrane coating, purified RBC membrane was first mixed with PLGA core at a protein-to-polymer weight ratio of 1:4, followed by bath sonication for 10 min. To prepare chitosan nanoparticles (Chi-NPs), 50 mL of PLGA (4 mg/mL in acetone) was added to 100 mL chitosan solution (1 mg/mL in water) under continuous stirring, followed by evaporation for 10 h.[28] For fluorescence labeling, DiD or DiO was mixed with PLGA polymer (dye-to-polymer weight ratio = 1:40,000) in acetone followed by nanoparticle preparation. RBC-NPs

or Chi-NPs were collected with centrifugation (19,000 ×g for 20 min). The pellets were washed with DI water three times to remove excess membrane or chitosan and re-dispersed in deionized water to a concentration of 20% w/v. The colloidal gel was prepared by mixing the two nanoparticle suspensions at desired ratios followed by a brief bath sonication of 3 min. The resulting NC-gel was stored at 4°C for further usage.

Characterization of NC-gel:

The rheological analysis was carried out at 25 ± 0.1°C on a strain-controlled AR-G2 rheometer with a 20 mm-diameter parallel-plate geometry (TA Instruments Inc., New Castle, DE). The 500 μm gap was filled with the 200 μL gel samples. A solvent trap was placed around the geometry to prevent liquid evaporation during the measurements. Oscillatory rheological measurements were performed in the linear viscoelastic region. The strain was kept at 0.03% and a dynamic frequency sweep from 0.1 to 10 rad/s was conducted to measure the storage modulus G' and loss modulus G''. The viscosity was monitored while the stress was increased (frequency = 1 Hz). Measurements were performed in triplicate with 10 min between cycles. The gel recoverability was assessed using no time break between cycles. For fluorescence imaging, 10 μL NC-gel was dropped onto the glass slide followed by covering it with a cover slip. The slide was then blocked with nail polish. The sample was imaged on Olympus FV1000 confocal microscope. To study hydrogel morphology, NC-gel was lyophilized and the flake of the gel was placed on a silicon wafer. The sample was coated with iridium and then examined with SEM (FEI XL30 SFEG).

RBC-NP retention study:

To study retention of RBC-NPs within the NC-gel, the RBC-NPs were labeled with a florescent dye DiD. The resulting NC-gel (500 μL) was loaded into a micro equilibrium dialyzer (Harvard Apparatus) and membrane filters (Whatman, nuclepore track-etch membrane) with the pore size of 1 μm in diameter were used for dialysis against 1 L water. At pre-determined time points, 250 μL of water outside of the chamber was taken and the fluorescence intensity was measured. RBC-NP suspension (10% w/v, 500 μL) without Chi-NPs were used as a control. RBC-NP retention was also studied in vivo. Specifically, prior to the study, the back of the mice (six week old male ICR mice from Envigo, n = 3) was carefully shaved. Then 50 μL DiD-labeled NC-gel was injected subcutaneously to the left flanks of the mice. As a control, RBC-NP suspension (10% w/v, 50 μL) without Chi-NPs was used and injected subcutaneously to the right flanks of the same mice. For live whole-body imaging, mice were anesthetized with isoflurane at designated time points (day 0, 1, 2, and 3) and imaged with a Xenogen IVIS 200 system. Fluorescence intensities were quantified and normalized across the time points. Heat maps were overlaid on bright field images. All animal experiments followed protocols that were reviewed, approved and performed under the regulatory supervision of the University of California, San Diego's institutional biosafety program and the Institutional Animal Care and Use Committee (IACUC).

Expression and purification of recombinant streptolysin O (SLO):

The *slo* gene was cloned into vector pET15b and transformed into BL21 DE3 *Escherichia coli*. Bacteria expressing SLO were cultured in 1 L of Luria-Bertani broth (LB) and

incubated at 37°C with shaking. Expression was induced in cultures at 0.7 A_{600} with 0.5 mm isopropyl 1-thio-β-D-galactopyranoside (Bio-Vectra) and maintained at 30°C for 4 h. Bacterial pellets were disrupted by sonication, and soluble 6× histidine-tagged SLO was purified using nickel-nitrilotriacetic acid-agarose (Invitrogen). Fractions corresponding to the full-length SLO were pooled and further purification was achieved using Amicon Ultra centrifugal filters (Millipore Sigma). Protein was monitored by SDS-PAGE and quantitated by A_{280} and frozen in aliquots at –80 °C. Assays were performed in the presence of 10 mm dithiothreitol (DTT) for reducing conditions.

Group A Streptococcus (GAS) culture:

GAS (M1 5448) bacteria were inoculated from a frozen stock to Todd-Hewitt agar plates and cultured for 12 h at 37°C. Following the culture, a single colony was selected and inoculated to 8 mL of Todd-Hewitt Broth (THB). After an overnight culture, 4 mL of the bacterial medium was reconstituted with 250 mL of fresh THB medium and the culture was continued until the optical density value at 600 nm (OD_{600}) reached 0.4, corresponding to 0.8×10^8 CFU/mL. The bacteria were then collected with centrifugation (4000 ×g for 5 min) and wash twice with PBS.

SLO neutralization study:

SLO hemolytic activity was first studied. 60 μL SLO (containing 10 mM DTT) with varied concentration was incubated with 0.1 mL 5% purified human RBCs at 37°C for 30 min. The concentration of SLO to induce 100% hemolysis were determined when the percentage of the released hemoglobin reached the same level as the lysate from the same amount of RBCs. To evaluate SLO neutralization by the NC-gel in vitro, 1.6 μL of SLO solution (0.1 mg/mL containing 10 mM of DTT) was mixed with 59 μL NC-gel, free RBC-NPs, and PBS, respectively. Then 0.1 mL of 5% purified human RBCs was added to each sample, followed by incubation at 37°C for 30 min. The samples were carefully centrifuged and the extent of RBC lysis was quantified by measuring the absorption of the supernatants at 540 nm. All experiments were performed in triplicate. To study neutralization of SLO by the NC-gel in vivo, 100 μL of SLO solution (0.6 mg/mL, containing 10 mM of DTT) was mixed with 100 μL of NC-gel and the mixture was injected subcutaneously into the flank region of 6 week-old male ICR mice (Envigo, n = 3). Three other groups, including SLO mixed with free RBC-NPs, SLO toxin alone, and PBS, were used as controls. After 72 h the lesion was photographed. Then the mice were sacrificed and the skin and muscle samples were removed. The tissues were frozen, cut, and stained with hematoxylin and eosin (H&E) for histological analysis (Hamamatsu Nanozoomer).

Antivirulence efficacy against localized GAS subutaneous infection:

Prior to the study, the flanks of 18 ICR mice (6 week old male, Envigo) were carefully shaved. Then a challenge dose of 2×10^9 CFU of GAS M1 5448 suspended in 100 μL PBS was injected subcutaneously into the flank region. Then the mice were randomly divided into three groups (n = 6 per group). For the treatment group, 0.1 mL NC-gel was injected into the infection region. For the control groups, free RBC-NPs or PBS were injected. The progression of infection in each mouse was carefully monitored and measured for 3 days, with serial photographic image capture and lesion size measurement using Image J software.

Acknowledgment

References

1. Zaccarelli E, Colloidal gels: equilibrium and non-equilibrium routes. J. Phys.: Condens. Matter 2007, 19, article number 323101.

2. Joshi YM, Dynamics of colloidal glasses and gels. Annu. Rev. Chem. Biomol. Eng 2014, 5, 181–202. [PubMed: 24655137]

3. Lu PJ; Weitz DA, Colloidal particles: crystals, glasses, and gels. Annu. Rev. Condens. Matter Phys 2013, 4, 217–233.

4. Kamata H; Li X; Chung UI; Sakai T, Design of hydrogels for biomedical applications. Adv. Healthc. Mater 2015, 4, 2360–2374. [PubMed: 25939809]

5. Gao WW; Zhang Y; Zhang QZ; Zhang LF, Nanoparticle-Hydrogel: A Hybrid Biomaterial system for localized drug delivery. Ann. Biomed. Eng 2016, 44, 2049–2061. [PubMed: 26951462]

6. Appel EA; Tibbitt MW; Webber MJ; Mattix BA; Veiseh O; Langer R, Self-assembled hydrogels utilizing polymer-nanoparticle interactions. Nat. Commun 2015, 6, article number 6295.

7. Diba M; Wang HN; Kodger TE; Parsa S; Leeuwenburgh SCG, Highly elastic and self-healing composite colloidal gels. Adv. Mater 2017, 29, article number 1604672.

8. Wang Q; Wang JX; Lu QH; Detamore MS; Berkland C, Injectable PLGA-based colloidal gels for zero-order dexamethasone release in cranial defects. Biomaterials 2010, 31, 4980–4986. [PubMed: 20303585]

9. Gu Z; Aimetti AA; Wang Q; Dang TT; Zhang YL; Veiseh O; Cheng H; Langer RS; Anderson DG, Injectable nano-network for glucose-mediated insulin delivery. ACS Nano 2013, 7, 4194–4201. [PubMed: 23638642]

10. Wang Q; Wang LM; Detamore MS; Berkland C, Biodegradable colloidal gels as moldable tissue engineering scaffolds. Adv. Mater 2008, 20, 236–239.

11. Wang Q; Gu Z; Jamal S; Detamore MS; Berkland C, Hybrid hydroxyapatite nanoparticle colloidal gels are injectable fillers for bone tissue engineering. Tissue Eng. Part A 2013, 19, 2586–2593. [PubMed: 23815275]

12. Kim BYS; Rutka JT; Chan WCW, Current concepts: nanomedicine. New Engl. J. Med 2010, 363, 2434–2443. [PubMed: 21158659]

13. Bobo D; Robinson KJ; Islam J; Thurecht KJ; Corrie SR, Nanoparticle-based medicines: a review of FDA-approved materials and clinical trials to date. Pharm. Res 2016, 33, 2373–2387. [PubMed: 27299311]

14. Hu CMJ; Zhang L; Aryal S; Cheung C; Fang RH; Zhang LF, Erythrocyte membrane-camouflaged polymeric nanoparticles as a biomimetic delivery platform. Proc. Natl. Acad. Sci. U. S. A. 2011, 108, 10980–10985. [PubMed: 21690347]

15. Hu CMJ; Fang RH; Copp J; Luk BT; Zhang LF, A biomimetic nanosponge that absorbs pore-forming toxins. Nat. Nanotechnol. 2013, 8, 336–340. [PubMed: 23584215]

16. Hu CMJ; Fang RH; Wang KC; Luk BT; Thamphiwatana S; Dehaini D; Nguyen P; Angsantikul P; Wen CH; Kroll AV; Carpenter C; Ramesh M; Qu V; Patel SH; Zhu J; Shi W; Hofman FM; Chen TC; Gao WW; Zhang K; Chien S; Zhang LF, Nanoparticle biointerfacing by platelet membrane cloaking. Nature 2015, 526, 118–121. [PubMed: 26374997]

17. Luk BT; Hu CMJ; Fang RNH; Dehaini D; Carpenter C; Gao WW; Zhang LF, Interfacial interactions between natural RBC membranes and synthetic polymeric nanoparticles. Nanoscale 2014, 6, 2730–2737. [PubMed: 24463706]

18. Fang RH; Hu CMJ; Luk BT; Gao WW; Copp JA; Tai YY; O'Connor DE; Zhang LF, Cancer cell membrane-coated nanoparticles for anticancer vaccination and drug delivery. Nano Lett 2014, 14, 2181–2188. [PubMed: 24673373]

19. Parodi A; Quattrocchi N; van de Ven AL; Chiappini C; Evangelopoulos M; Martinez JO; Brown BS; Khaled SZ; Yazdi IK; Vittoria Enzo M; Isenhart L; Ferrari M; Tasciotti E, Synthetic nanoparticles functionalized with biomimetic leukocyte membranes possess cell-like functions. Nat. Nanotechnol 2013, 8, 61–68. [PubMed: 23241654]

20. Gao WW; Fang RH; Thamphiwatana S; Luk BT; Li JM; Angsantikul P; Zhang QZ; Hu CMJ; Zhang LF, Modulating antibacterial immunity via bacterial membrane-coated nanoparticles. Nano Lett 2015, 15, 1403–1409. [PubMed: 25615236]

21. Gao WW; Zhang LF, Engineering Red blood cell membrane-coated nanoparticles for broad biomedical applications. AICHE J. 2015, 61, 738–746.

22. Hu CMJ; Fang RH; Luk BT; Zhang LF, Nanoparticle-detained toxins for safe and effective vaccination. Nat. Nanotechnol 2013, 8, 933–938. [PubMed: 24292514]

23. Wei X; Gao J; Wang F; Ying M; Angsantikul P; Kroll AV; Zhou J; Gao W; Lu W; Fang RH; Zhang L, In Situ Capture of bacterial toxins for antivirulence vaccination. Adv. Mater 2017, 29, article number 1701644.

24. Chen WS; Zhang QZ; Luk BT; Fang RH; Liu YN; Gao WW; Zhang LF, Coating nanofiber scaffolds with beta cell membrane to promote cell proliferation and function. Nanoscale 2016, 8, 10364–10370. [PubMed: 27139582]

25. Li LL; Xu JH; Qi GB; Zhao XZ; Yu FQ; Wang H, Core-shell supramolecular gelatin nanoparticles for adaptive and "on-demand" antibiotic delivery. ACS Nano 2014, 8, 4975–4983. [PubMed: 24716550]

26. Wang F; Gao WW; Thamphiwatana S; Luk BT; Angsantikul P; Zhang QZ; Hu CMJ; Fang RH; Copp JA; Pornpattananangkul D; Lu WY; Zhang LF, Hydrogel retaining toxin-absorbing anosponges for local treatment of methicillin-resistant *Staphylococcus aureus* infection. Adv. Mater 2015, 27, 3437–3443. [PubMed: 25931231]

27. Copp JA; Fang RH; Luk BT; Hu CMJ; Gao WW; Zhang K; Zhang LF, Clearance of pathological antibodies using biomimetic nanoparticles. Proc. Natl. Acad. Sci. U. S. A. 2014, 111, 13481–13486. [PubMed: 25197051]

28. Wang Q; Jamal S; Detamore MS; Berkland C, PLGA-chitosan/PLGA-alginate nanoparticle blends as biodegradable colloidal gels for seeding human umbilical cord mesenchymal stem cells. J. Biomed. Mater. Res. A 2011, 96A, 520–527.

29. Gao WW; Vecchio D; Li JM; Zhu JY; Zhang QZ; Fu V; Li JY; Thamphiwatana S; Lu DN; Zhang LF, Hydrogel containing nanoparticle-stabilized liposomes for topical antimicrobial delivery. ACS Nano 2014, 8, 2900–2907. [PubMed: 24483239]

30. Walker MJ; Barnett TC; McArthur JD; Cole JN; Gillen CM; Henningham A; Sriprakash KS; Sanderson-Smith ML; Nizet V, Disease manifestations and pathogenic mechanisms of group A Streptococcus. Clin. Microbiol. Rev 2014, 27, 264–301. [PubMed: 24696436]

31. Buffalo CZ; Bahn-Suh AJ; Hirakis SP; Biswas T; Amaro RE; Nizet V; Ghosh P, Conserved patterns hidden within group A Streptococcus M protein hypervariability recognize human C4b-binding protein. Nat. Microbiol 2016, 1, article number 16155.

32. Stewart CM; Buffalo CZ; Valderrama JA; Henningham A; Cole JN; Nizet V; Ghosh P, Coiled-coil destabilizing residues in the group A *Streptococcus* M1 protein are required for functional interaction. Proc. Natl. Acad. Sci. U. S. A. 2016, 113, 9515–9520. [PubMed: 27512043]

33. Humar D; Datta V; Bast DJ; Beall B; De Azavedo JCS; Nizet V, Streptolysin S and necrotising infections produced by group G *Streptococcus*. Lancet 2002, 359, 124–129. [PubMed: 11809255]

34. Zhu H; Liu MY; Sumby P; Lei BF, The secreted esterase of group A *Streptococcus* is important for invasive skin infection and dissemination in mice. Infect. Immun 2009, 77, 5225–5232. [PubMed: 19805529]

35. Kim J; Li WA; Choi Y; Lewin SA; Verbeke CS; Dranoff G; Mooney DJ, Injectable, spontaneously assembling, inorganic scaffolds modulate immune cells in vivo and increase vaccine efficacy. Nat. Biotechnol 2015, 33, 64–72. [PubMed: 25485616]
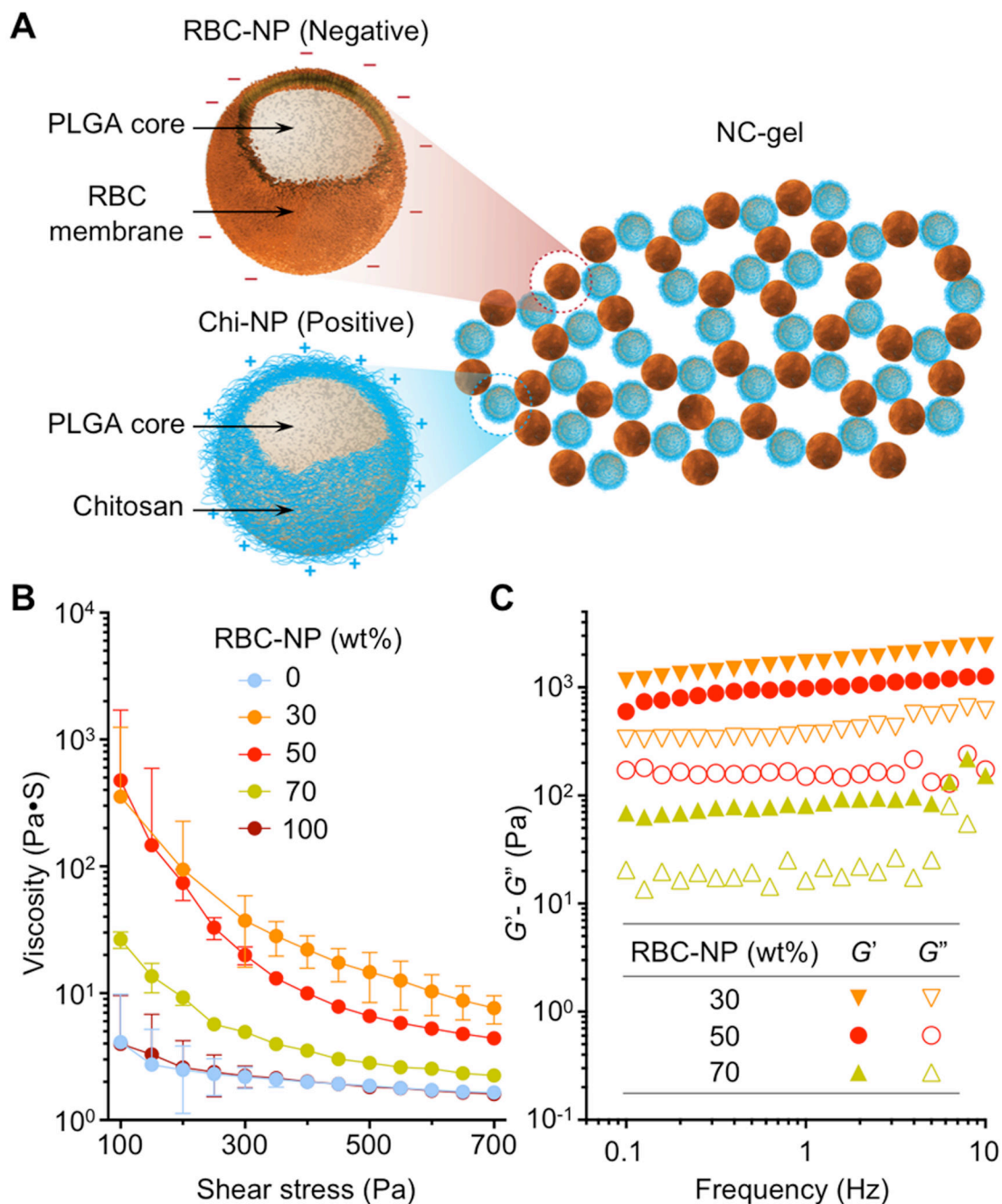
Figure 1. Preparation of nanosponge colloidal gel (denoted 'NC-gel').
(A) Schematic illustration of NC-gel formulation by mixing red blood cell membrane-coated nanoparticles (RBC-NPs), which possess a negative surface charge, with chitosan-modified nanoparticles (Chi-NPs) as positively charged nanoparticle counterparts. (B) RBC-NPs and Chi-NPs mixed at different mass ratios (0, 30, 50, 70, and 100 wt% of RBC-NP, respectively) were measured for viscosity with varying shear stress (100–700 Pa). (C) RBC-NPs and Chi-NPs mixed at different mass ratios (30, 50, and 70 wt% of RBC-NP, respectively) were measured for the storage modulus G' and loss modulus G'' against frequency (0.1–10 Hz). All rheological measurements were performed at 25°C.
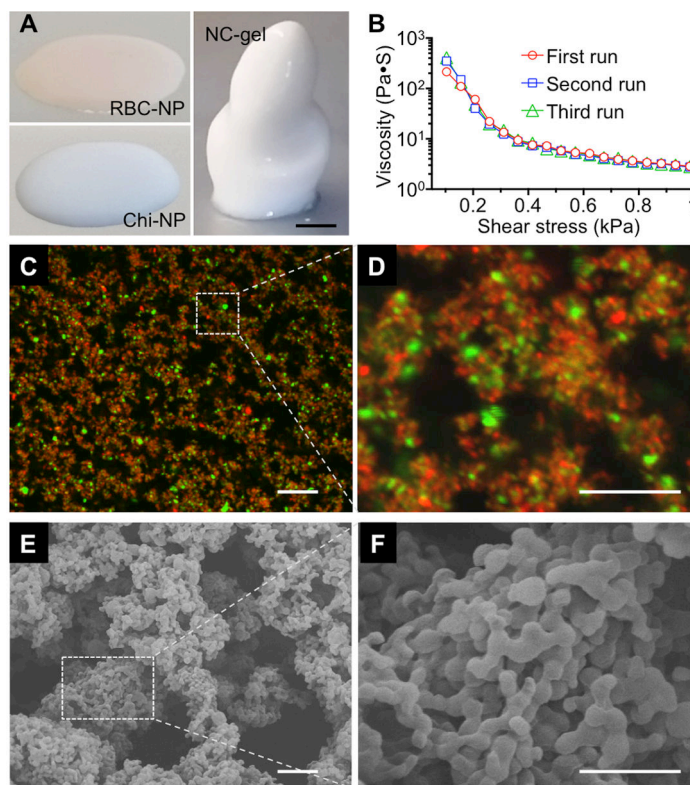
Figure 2. Characterization of the NC-gel.
(A) Images of RBC-NPs, Chi-NPs, and NC-gel samples when they were placed onto a flat substrate. Scale bar = 5 mm. (B) Viscosity measurements were performed on the same NC-gel sample at 25°C for three consecutive runs without interval between each run. (C) A representative fluorescence image of the NC-gel, in which RBC-NPs were labeled with DiD dye (red) and Chi-NPs with DiO dye (green). Scale bar = 1 μm. (D) A zoomed-in image of the marked area in (C). Scale bar = 10 μm. (E) A representative scanning electron microscopy (SEM) image of NC-gel. Scale bar = 1 μm. (F) A zoomed-in SEM image of the marked area in (E). Scale bar = 0.5 μm.
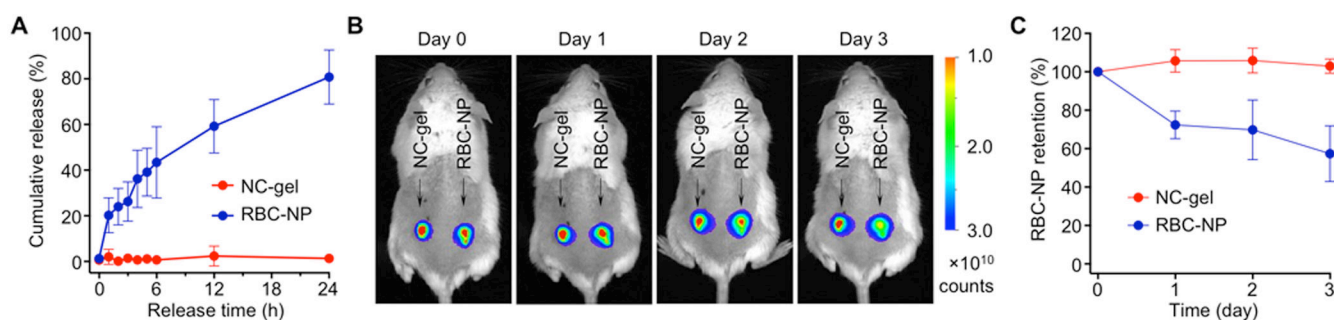
Figure 3. RBC-NP retention within the NC-gel.
(A) The cumulative release of RBC-NPs measured from the NC-gel and RBC-NP suspension, respectively. RBC-NP was labeled with DiD dye and samples were placed in dialysis chambers equipped with filters of pore size of 1 μm. (B) Fluorescence images of mice injected with NC-gel and RBC-NP samples. NC-gel was formulated with DiD-labeled RBC-NPs. The samples were injected subcutaneously under the loose skin over the left flank of the mice. RBC-NPs alone without mixing with Chi-NPs were injected as a control over the right flank of the same mice. Fluorescence images were taken on day 0, 1, 2, and 3 after the injection. (C) Quantification of the fluorescence intensity as observed in (B). All images are representative of three mice from each group and error bars represent the standard deviation (n = 3).
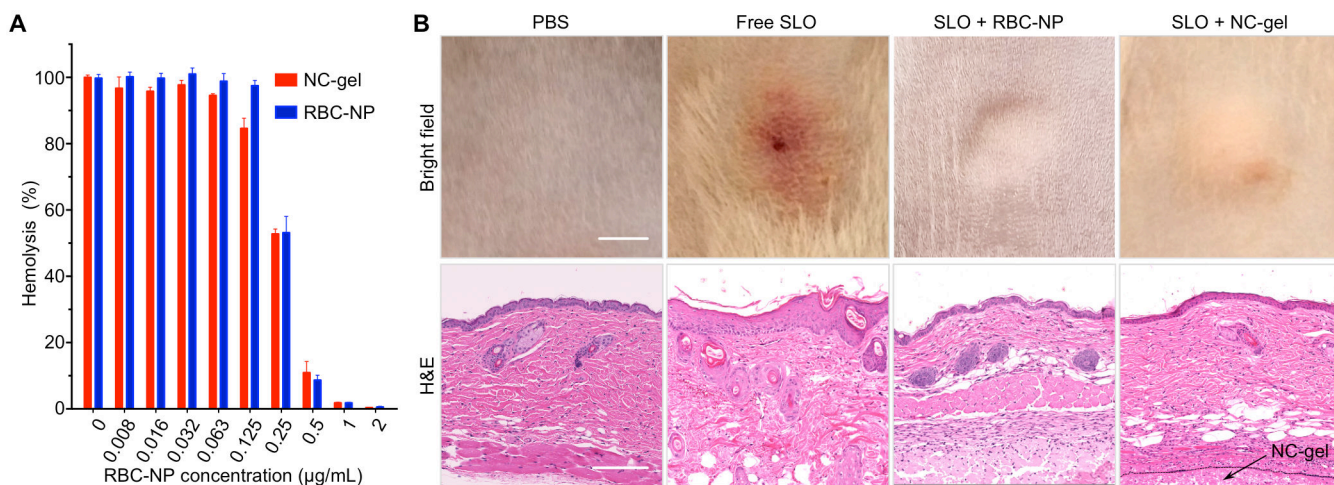
Figure 4. Evaluation of toxin neutralization capability of the NC-gel in vitro and in vivo.
(A) In vitro neutralization of *Streptolysin*-O (SLO) by the NC-gel and free RBC-NPs to inhibit toxin-induced hemolysis. In all samples, SLO concentration was maintained at 1 µg/mL and the concentration of RBC-NP component was varied. (B) In vivo neutralization of SLO. Free SLO, SLO+RBC-NP, or SLO+NC-gel was injected subcutaneously into CD-1 mice. Mice injected with PBS only served as a control group. Mice injected with free SLO developed skin lesions after 3 days, but no lesions were observed for mice in other treatment groups (scale bar = 20 mm). Hematoxylin and eosin (H&E) stained histological sections revealed inflammatory infiltrate, apoptosis, necrosis, and edema in the epidermis for the SLO-treated mice. In contrast, mice in other groups showed no abnormality in the epidermis (scale bars = 0.2 mm).
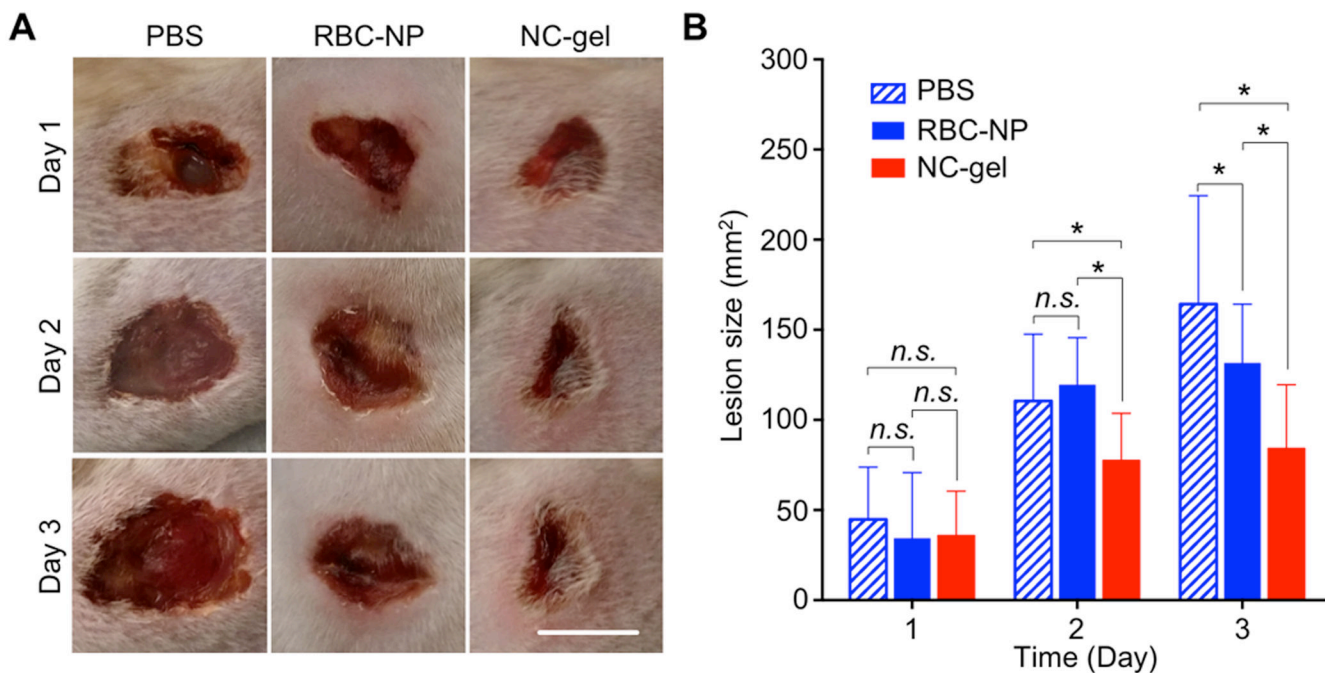
Figure 5. Evaluation of the NC-gel for protecting mice from group A *Streptococcus* (GAS) infection in vivo.

To establish GAS infection, 2×10^9 CFU of GAS bacteria were injected subcutaneously under the loose skin on the back of the mice (n = 6 per group). Immediately after injection of the bacteria, PBS, RBC-NP alone, or NC-gel was injected to the infection site. (A) Skin lesions were monitored and photographed on day 1, 2, and 3 after the injection (scale bar = 1 cm). (B) The lesion sizes were measured and compared among the groups. Bars represent median values (*: $P < 0.05$, *n.s.*: not significant).